

The Dark and Luminous Matter coupling in the formation of spheroids: a SPH investigation

Cesario Lia¹, Giovanni Carraro² and Paolo Salucci¹

¹ SISSA/ISAS, via Beirut 2, I-34013, Trieste, Italy

² Department of Astronomy, Padova University, vicolo dell'Osservatorio 5, I-35122, Padova, Italy

e-mail: liac@sisssa.it, carraro@pd.astro.it

Received February 16; accepted

Abstract. Using N-body/hydrodynamical simulations which include prescriptions for Star Formation, Feed-Back and Chemical Evolution, we explore the interaction between baryons and Dark Matter (DM) at galactic scale. The N-body simulations are performed using a Tree-SPH code that follows the evolution of individual DM halos inside which stars form from cooling gas, and evolve delivering in the interstellar medium (ISM) mass, metals, and energy.

We examine the formation and evolution of a giant and a dwarf elliptical galaxy of total mass $10^{12}M_{\odot}$ and 10^9M_{\odot} , respectively.

Starting from an initial density profile like the universal Navarro et al (1996) profile in the inner region, baryons sink towards the center due to cooling energy losses. At the end of the collapse, the innermost part ($\simeq 1/20$ of the halo size) of the galaxy is baryon-dominated, whereas the outer regions are DM dominated.

The star formation proceeds at a much faster speed in the giant galaxy where a spheroid of $8 \times 10^{10}M_{\odot}$ is formed in 2 Gyr , with respect to the dwarf galaxy where the spheroid of $2 \times 10^7M_{\odot}$ is formed in 4 Gyr . For the two objects the final distributions of stars are well fitted by a Hernquist profile with effective radii of $r_e = 30\text{ kpc}$ and 2.8 kpc , respectively. The dark-to-luminous transition radius r_{IBD} occurs roughly at $1\text{ }r_e$, as in real ellipticals. The DM halo density evolution is non-adiabatic and does not lead to a core radius.

Key words: Galaxy formation – Dark Matter – Nbody simulation

1. Introduction

Galaxies of any morphological type and luminosity are known to be surrounded by DM halos, whose properties are remarkably universal (Salucci & Persic 1997 and references therein). The presence of DM halos has been detected through a variety of observational methods (Danziger 1997), going from rotation curves in spirals (Giraud 2000, Swaters 1999, Persic et al 1996) to M/L ratios in ellipticals (Bertola et al 1993, Loewenstein & White III 1999 and references therein). To summarize, the properties of DM halos can be described as follows (Salucci & Persic 1997):

- dark and visible matter are well mixed already inside the luminous region of the galaxy;
- the transition radius R_{IBD} between the inner, baryon dominated region, and the outer, DM dominated region, moves inward progressively with decreasing luminosity;
- a halo core radius, comparable with the optical radius, is detected at all luminosities and for all morphologies;
- the luminous mass fraction varies with luminosity in a fashion common to all galaxy types: it is comparable with the cosmological baryon fraction at $L \simeq L_{\star}$, but it decreases by about a factor 100 at $L \ll L_{\star}$;
- finally, for any Hubble type, the central halo density increases with decreasing luminosity.

Attempts to model the properties of DM halos in a cosmological context with N-body simulations trace back to Dubinski & Carlberg (1991) in the frame of Cold Dark Matter (CDM) theory. The halos were found to be strongly triaxial and to exhibit a power law density profile varying from -1 in the center to -4 in the outskirts (Hernquist 1990 profile). Then, Navarro et al (1996) (hereafter NFW), found that, independently from the adopted initial perturbation spectrum, the cosmological model and

Send offprint requests to: G. Carraro (carraro@pd.astro.it)

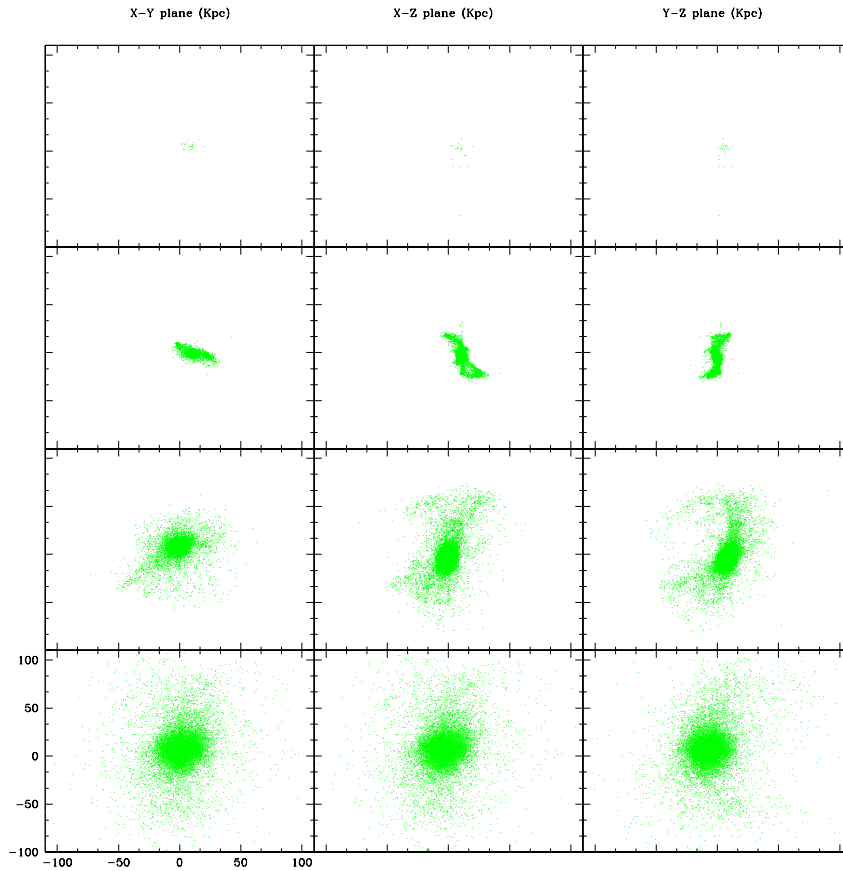


Fig. 1. The formation of a giant elliptical. From the top to the bottom, snapshots refer to 1, 2, 3 and 9 Gyrs.

the halo mass, all DM halos possess the same *universal* density profile, fitted by the formula

$$\frac{\rho_r}{\rho_{crit}} = \frac{\delta_c}{(r/r_s)^a (1 + r/r_s)^{3-a}}, \quad (1)$$

where $a = 1$, $\rho_{crit} = 3H_o^2/8\pi G$ is the critical density for closure, δ_c is a dimensionless characteristic density, and r_s is a scale radius, which defines where the profile shape has slope -2 .¹

This profile has a spike in the center of the halo, and differs in its asymptotic behavior from the Hernquist profile, decreasing as r^{-3} far from the halo center. Other simulations, with higher resolution and/or different initial conditions, confirmed the basic features of these findings, but disagreed in some important aspects (Cole & Lacey 1996, Moore et al 1997, van der Bosh, 1999). In fact, there

are claims that the *universality* of the functional form (1) arises as a direct consequence of the hierarchical merging history of CDM halos (Syer & White (1997), or as a more generic feature of gravitational collapse (Huss et al. 1998). However, recently, the steepness of the central cusp has been found to significantly vary among different realizations, i.e. among halos (Jing & Suto 2000). It seems now likely that, CDM halos follow eq (1) with $a \simeq 1.5$ but with large variations of r_s with mass and also at a given halo mass.

On the other hand, there exists a large discrepancy between CDM halo predictions and DM observations (Salucci & Persic 1997). Halos around galaxies show a density distribution inconsistent with eq (1). In particular, they have a density central core larger than the stellar

¹ * We take as Hubble's constant $H_o = 75 \text{ Km/sec/Mpc}$.

$$\rho_h(r) \propto \frac{1}{(r + r_0)(r_0^2 + r^2)}$$

with $r_0 \gg r_e$, r_e being the effective radius.

The disagreement between theory and observations on the mass distribution, and the existence of global scaling laws that couple the dark and the luminous matter (Persic et al 1996) prompt the investigation of the past dynamical history of galaxies.

N-body/hydrodynamical simulations are an effective tool to obtain crucial information on the late stages of galaxy formation in some sense orthogonal to that we obtain with semi-analytical methods or we infer from observations. In fact, such simulations can account for the "physical" interaction between gas and dark matter. Moreover, many relevant physical processes occurring in the baryonic components, like thermal shocks, pressure forces and dissipation are explicitly taken into account.

The layout of the paper is as follow. In Section 2 we briefly describe the numerical tool, in Section 3 we discuss the initial conditions. In Section 4 and 5 we show the evolution of a giant and a dwarf elliptical, respectively. Finally, Section 6 summarizes the results.

2. The CODE

The simulations we present here have been performed by means of the Tree-SPH code developed by Carraro (et al 1998), Buonomo et al (2000) and Lia & Carraro (2000). The code, which is able to follow the evolution of a mix of CDM and Baryons (gas and stars), has been successfully checked against standard tests in Carraro et al. (1998), while a fine exploration of the parameters space is presented in Buonomo et al (2000).

In detail, the gas component is "followed" by means of the Smoothed Particle Hydrodynamics (SPH) technique (Lucy 1977; Gingold & Monaghan 1997; Hernquist & Katz 1989; Steinmetz & Müller 1993), while the gravitational forces are taken into account by means of the hierarchical tree algorithm of Barnes & Hut (1986). In detail, we adopt a tolerance parameter $\theta = 0.8$, a Plummer softening parameter and we expand the tree nodes to quadrupole order.

In SPH each particle represents a fluid element whose position, velocity, energy, density etc. are followed in time and space. The properties of the fluid are locally estimated by an interpolation which involves the smoothing length h_i . Each particle possesses its own time and space variable smoothing length h_i , and evolves with its own time-step. This renders the code highly adaptive and flexible, and suited for numerical "experiments".

Radiative cooling is considered as a function of temperature and metallicity following Sutherland & Dopita (1994) and Hollenbach & McKee (1979) : the code takes into account the variations in metallicity among the fluid

Star Formation (SF) and Feed-back algorithms are described in Buonomo et al (2000). Specifically SF, following partly Katz (1992), is set to occur when

$$t_{sound} > t_{ff}$$

and

$$t_{cooling} < t_{ff}$$

with the star formation rate of

$$SFR = \frac{d\rho_*}{dt} = -\frac{d\rho_g}{dt} = \frac{c_*\rho_g}{t_g}$$

where c_* is the dimensionless efficiency of star formation, and t_g is the characteristic time for the gas to flow, usually set to the maximum between the cooling time and the free-fall time. For the simulations here discussed we keep $c_* = 1.0$. When formed, stars are distributed in mass according to the Miller & Scalo (1979) Initial Mass Function (IMF).

The effects of energy (and mass) feed-back from supernovae and stellar winds are also taken into account (Chiosi & Maeder 1986, Thornton et al 1998). In this experiments we deposit all the energy released by SNæ ($10^{49}erg$) and stellar wind in the thermal budget of the bubble, following the kind of arguments discussed in Buonomo et al (2000).

Finally, the chemical enrichment of the interstellar gas caused by the the stellar wind and ejecta is followed by means of the closed-box model applied to each gas-particle as in Carraro et al. (1998). Metals are then SPH-diluted over the surrounding gas particles.

3. Initial conditions

The code follows the dynamical formation of galaxies since the moment in which the protohalo detaches itself from the Hubble flow with its cosmological share of baryonic material. Then, we set *ad hoc* initial configuration for a protogalaxy and let the system evolve within the SPH scheme above described. Moreover, we assume that the star formation starts after the dark halo is virialized.

This approach is justified on the grounds that in this paper, we are aimed at 1) testing a simple but reasonable initial conditions set-up and 2) focusing on processes which occur mainly at scales much smaller than the halo virial radius.

The working scenario is that, after a violent relaxation process, which follows the separation from the Hubble expansion, the DM halo acquires a particular density distribution, and then it accretes baryonic material which heats up to the halo virial temperature. Gas then radiatively cools and collapses, and through fragmentation turns into the stars we see today in disks and spheroidal systems.

This scenario is not incompatible with the merging one, withstanding that the baryonic collapse takes place after the last merging episode.

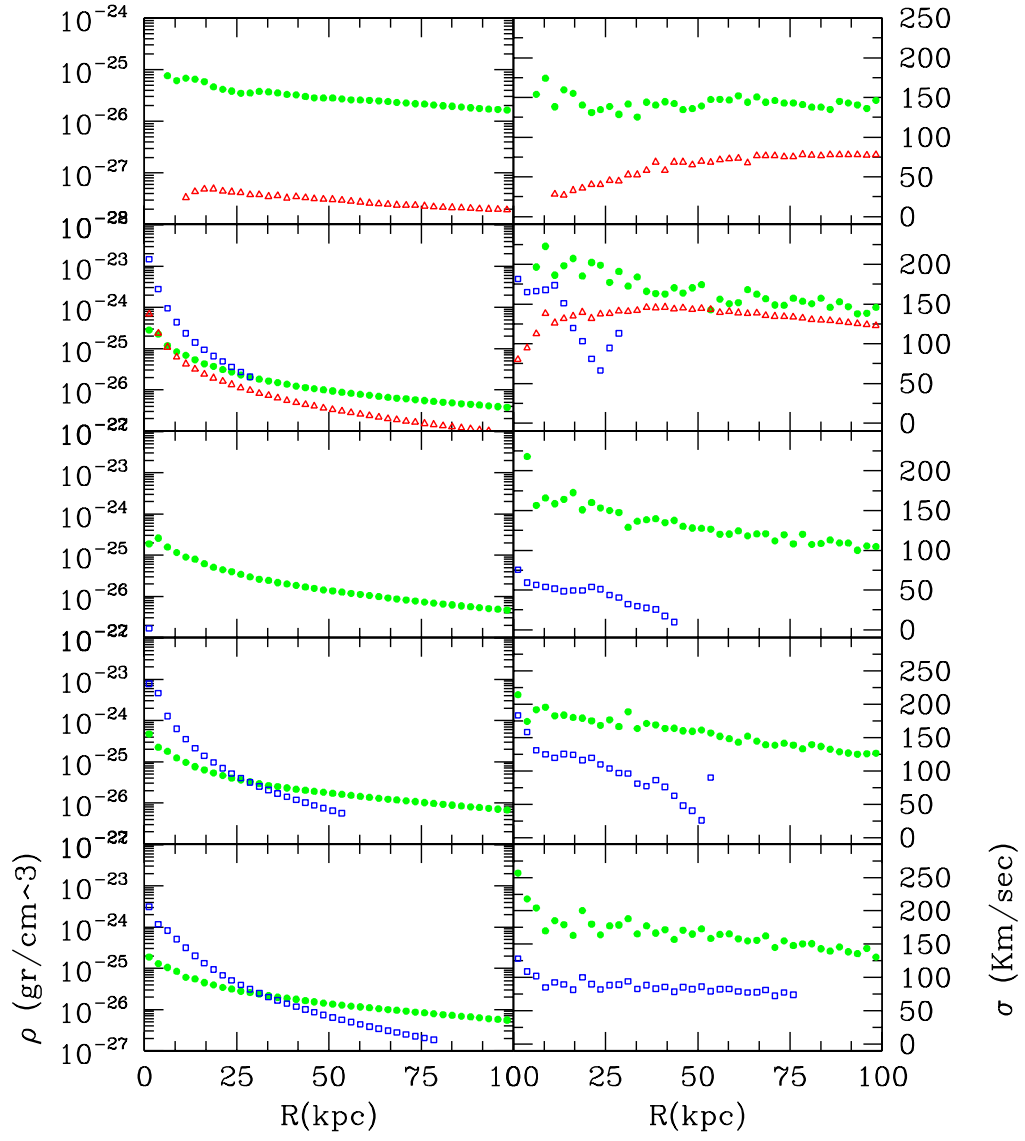


Fig. 4. Time evolution of the density and dispersion profiles. Solid circles stand for DM, open triangles for gas and open squares for stars. From the top to the bottom profiles refer to 1, 3, 3.5, 4.5 and 9 Gyr.

4. Initial configuration

We set up a protogalaxy as an isolated virialized DM halo with baryonic material inside it. We assume spherical, isotropic and non-rotating halos of density profiles:

$$\rho(r) \propto \frac{1}{r}. \quad (2)$$

Let us notice that eq. (2) matches the profile of CDM halos in the innermost regions, especially in low Ω Universe for which $r_s \sim 10 - 30$ kpc. Different profiles, more in line with observations or theoretical claims, will be considered in forthcoming papers.

Gravitational interaction is modeled by adopting a Plummer softening constant over the simulation and equal for both DM and gas. By plotting the inter-particles separation as a function of the galactocentric distance, we derive the softening parameter ϵ as the mean inter-particles separation at the center of the sphere, taking at least one hundred particles inside the softening radius.

DM particles (10,000 in number) are distributed inside a sphere according to an *acceptance-rejection* procedure for generating random deviations with a known distribution function (Press et al 1989).

persion velocity $\sigma(r)$ according to:

$$\sigma^2(r) \propto (r \ln(\frac{1}{r})). \quad (3)$$

which is the solution of the Jeans equation for spherical isotropic collisionless system with the density profile of eq (2).

Fixing the total mass of the system M_{200} , we assume that a radius

$$R_{200} \equiv (\frac{3}{4\pi})^{1/3} (\frac{M_{200}}{200\rho_c})^{1/3} \gg r_e$$

truncates the dark halo, where ρ_c is the critical density to close the Universe.

Table 1. Properties of the virialised primordial DM halos.

$Mass$	T_{vir}	R_{200}
$10^{10} M_\odot$	$10^5 \text{ } ^\circ K$	kpc
100	3.8	256
0.1	1.2	35

The systems are then let to evolve until virial equilibrium is reached. 10,000 baryonic particles are then homogeneously distributed inside the DM halo with zero velocity field and low metal content ($Z = 10^{-4}$). The initial gas temperature is $10^4 \text{ } ^\circ K$.

5. A Giant Elliptical Galaxy

In the first simulation we set a giant elliptical of gaseous mass of $10^{11} M_\odot$ to form through the collapse of a spherical DM halo of $10^{12} M_\odot$. Each gas particle has an initial mass of $10^7 M_\odot$.

Looking at Figs. 1 and 2, baryons slowly infall towards the center of the potential well, gas condenses, cools and then finally stars begin to form at a rate of $50 M_\odot yr^{-1}$. The strong episode of star formation lasts for about 2 Gyr and it is marked by a large rate of production of SNæ of type II. These, however, are not able to expel from the galaxy a relevant fraction of the gas, given its strong gravitational field. At the end of this period, it has been processed into stars 80% of the original material. The remaining 20% is left partly in the outermost regions of the dark halo, partly out of the virial radius.

The collapse of baryons in the DM potential well can be realized by noticing that, at $t = 0$, in the innermost 10 kpc of the protogalaxy, the DM halo is 10 times denser than the gaseous component but at the end of the formation of the spheroid, the stellar component reaches a "central" density 30 times that of the dark component.

Not surprisingly, the final distribution of stars does not follow that of the DM. In fact, as the infall proceeds, the

C^1 scale r_e of about one tenth of the virial radius. More precisely, the dissipative zero-angular momentum infall of the (out-to-250 kpc) scale-free baryonic material produces a half-mass scale-length of ~ 30 kpc. The final stellar distribution closely follows a Hernquist profile (see Fig. 3) with effective radius r_e slightly larger than that of ellipticals of the same baryonic mass. However, the simulated value of r_e depends on the assumed DM density and on the prescriptions of star formation. Actually, one could use the observed r_e vs stellar mass relationship to fine-tune the semi-analytical parts of the code (Buonomo et al 2000).

During the galaxy assembly there creates a coupling between the baryons and the DM. The initial halo distribution $\rho(r, 0) = M_{200}/(2\pi R_{200}^2)1/r$ gets first slightly contracted by the baryonic infall and then expanded back by a (limited) supernovae-driven outflow. As result, the final DM distribution is not too different from the primordial one. On the other side, the DM potential controls the star formation rate and efficiency, including the fate of stellar ejecta.

Even in the present simplified scenario, the time-evolution of the mass distribution is not that of an adiabatic process (Blumenthal et al 1986). In fact, (see Fig. 5) the adiabatic invariant $rM(r)$ varies with time. In the innermost parts $r < 50$ kpc, it increases with time while, for larger radii, $r < 100$ kpc, it decreases as the collapse proceeds. The baryonic infall develops shell crossings as effect of the strong radial dependence of the the energy (un)balance among cooling, heating and release of gravitational energy.

6. A Dwarf Elliptical Galaxy

The second simulation concerns a proto-elliptical of gaseous mass of $10^8 M_\odot$ forming through the monolithic collapse of a spherical virialized DM halo of $M_{200} = 10^9 M_\odot$. In this case a gas particle has an initial mass of $10^4 M_\odot$.

Despite the virial radius is now much smaller ($R_{200} = 35$ kpc) the gas is not more rapid in condensating, cooling and forming stars. Notice that both the free-fall time and the cooling time are smaller.

The time evolution of the SFR in this case cannot be described as a single burst, but rather as a series of several episodes, each one of about $0.5 - 1 M_\odot yr^{-1}$, lasting for over 4 Gyr (see Figs. 6 and 7), a result which is in close agreement with observations of Dwarf Galaxies in the Local Group (Mateo 1998).

At the end of this period it has been processed into long-living stars only 20% of the original material. The remaining has been thrown out from the galaxy or left,

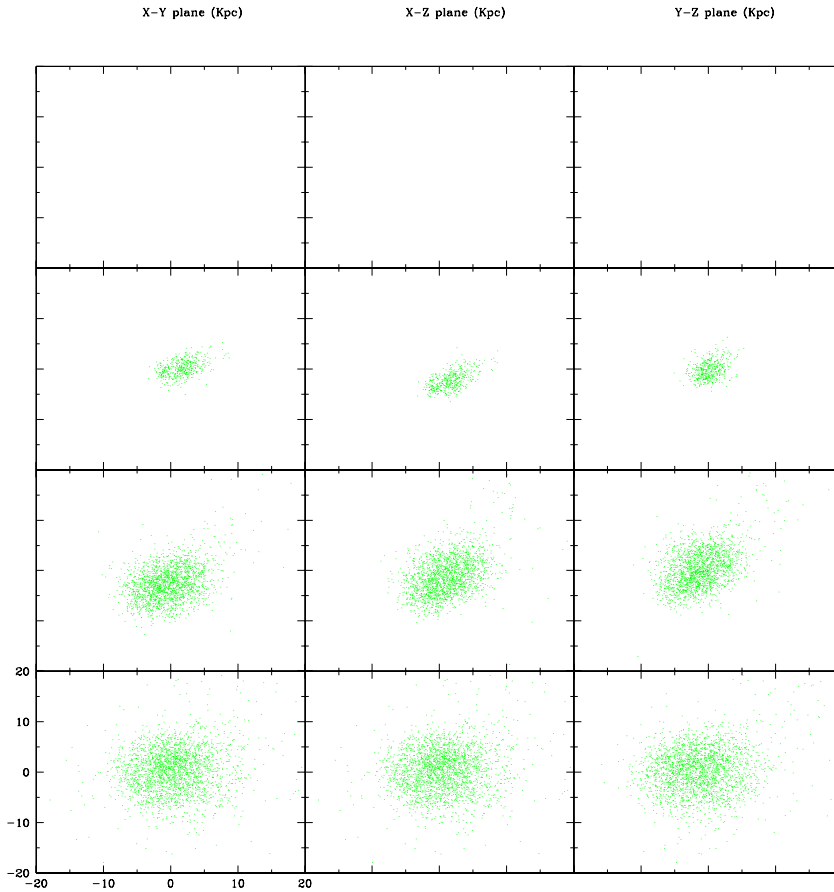


Fig. 5. The formation of a dwarf elliptical. From the top to the bottom, snapshots refer to 1, 2, 3 and 9 Gyrs.

unprocessed, behind, in the outermost regions of the DM halo.

In the central regions, the baryonic density increases as the collapse proceeds to reach "at the center" 30 times the density of the dark component. The stellar scale-length is $r_e \sim 2.8$ kpc not too different from that of ellipticals of the same baryonic mass (see Fig.8). Also in this case there is a clear coupling between baryons and DM during the galaxy assembly.

However, in this case, due to the weaker gravitational field, most of the gas gets expelled from the galaxy. The halo density evolves during the baryonic infall, in a non-adiabatic way, as shown in Fig. 9. The final DM distribution is not too different from the primordial one (see Fig. 10).

7. Discussion and Conclusions

In this paper we have investigated the coupling between DM and baryons during an assumed monolithic formation of two galaxies: a giant and a dwarf spheroidal galaxy. Starting from a homogeneous distribution, baryons sink toward the center of the virialized DM halo due to cooling instability. The smallest object has about 10 independent episodes of star formation 0.3 *Gyr* long, while the largest has basically one single burst 10 times longer. This difference nicely matches the available observations. Giant elliptical galaxies are indeed old objects dominated by a single burst of star formation (Bender et al 1992), whereas dwarf ellipticals exhibit basically an irregular and intermittent SF history (Mateo 1998). A crucial and sensitive aspect of our simulations is that both the giant and the dwarf object have been modeled with the same number of particles, which implies an increase by a factor 10^3 in the mass resolution passing from

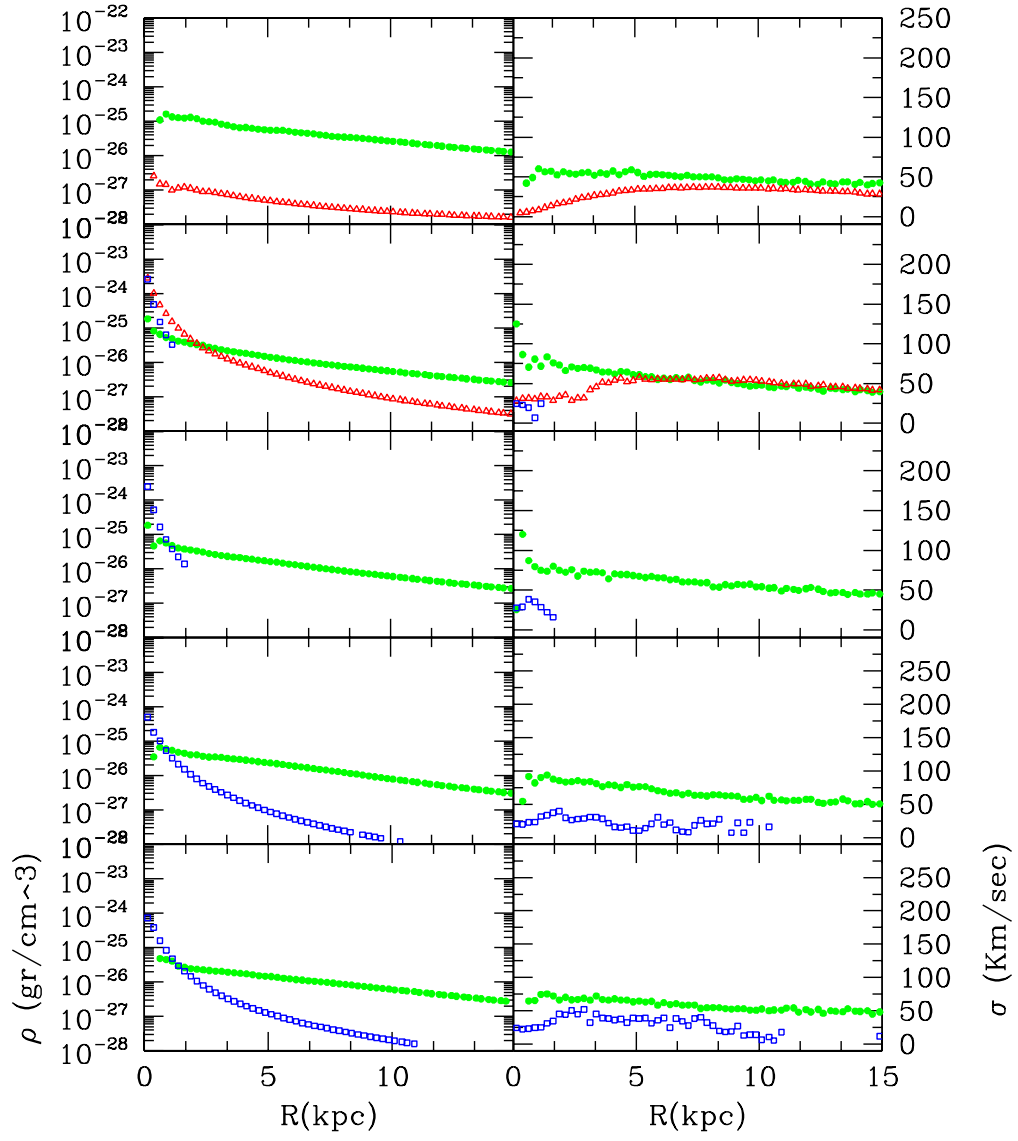


Fig. 9. Evolution of density and dispersion profiles for the Dwarf Elliptical Galaxy. Solid circles stand for DM, open triangles for gas and open squares for stars. From the top to the bottom profiles refer to 1.5, 2, 3.5, 5 and 9 Gyr.

the giant to the dwarf.

To check whether the results for the SF histories depend on the mass resolution of our simulations, the giant galaxy has been re-simulated using 2,000, 20,000 and 200,000 particles, whilst the dwarf galaxy has been re-simulated using 2,000 and 20,000 particles. This way the mass resolution goes from 10^8 to $10^6 M_\odot$ for the giant galaxy, and from 10^5 to $10^4 M_\odot$ for the dwarf galaxy. The results are summarized in Fig. 2 and Fig. 7, where we compare the SF histories of the two galaxy models at increasing mass resolution.

In both cases we show a reasonable convergence of the results.

As for the giant galaxy (see Fig. 2), we show that the SF history is dominated by a single ancient burst of SF, whose trend does not change too much passing from 2,000 to 200,000 particles. Nevertheless a more careful analysis shows that a difference emerges passing from 2,000 to 20,000 particles, whereas passing from 20,000 to 200,000 particles does not change significantly the global result. Although the SF peak is almost the same in all the simulations, the low resolution run produces a burst larger than the other two cases. Correspondingly the amount of gas

90% in the low resolution run to about 80% in the medium and high resolution run. This means that at increasing number of particles the results asymptotically converges. These conclusions confirm previous analysis on the performances of the SPH method (Steinmetz & Müller 1993, Thacker et al 1999). By comparing different SPH implementations they find that the minimum number of particles required to calculate local physical variables in dynamically evolving systems is about 10,000, and that the SPH method can give reasonable results also by using a small number of particles.

On the other hand, changing the resolution by a factor 10 does not alter the SF history of the dwarf galaxy (see Fig. 7), which exhibits several episodes of SF, although the number and position of the peaks does not coincide exactly.

The basic results of this paper can be summarized as follows:

- the stars which are formed show a final distribution much different from the DM distribution and can be represented by a Hernquist profile with a length-scale r_e ;
- a particular aspect of the mass distribution is that the regions inside r_e , are baryon dominated, while the DM is the main mass component at outer radii, as observed in real ellipticals;
- finally is worth noticing that, in both objects, the final DM velocity dispersion is about 1-2 times the stars velocity dispersion, in agreement with Loewenstein & White III (1999) findings.

In forthcoming papers we are going to analyze simulations which adopt different initial conditions for DM, in order to test the effect of the DM initial properties (density profile, velocity dispersion and so forth) on the final baryon distribution.

8. Acknowledgments*

The authors acknowledge very useful discussion with dr. E. Pignatelli and Prof. L. Danese. Moreover we thanks an anonymous referee for his detailed comments on the first version of this paper. We acknowledge financial support from Italian Ministry of Research, University, Science and Technology (MURST).

References

Barnes J. E., Hut P., 1986, *Nature* 324, 446
 Bender R., Burstein D., Faber S.M., 1992, *ApJ* 399, 462
 Bertola F., Pizzella A., Persic M., Salucci P., 1993, *ApJ* 416, L45
 Blumenthal G.R., Faber S.M., Flores R., Primack J.R. 1986, *ApJ* 301, 27

371
 Carraro G., Lia C., Chiosi C., 1998, *MNRAS* 298, 1021
 Chiosi C., Maeder A., 1986, *ARA&A*, 24, 329
 Cole S., Lacey C., 1997, *MNRAS* 281, 716
 Danziger I.J., 1997, in "Dark and Visible Matter in Galaxies", Persic M. & Salucci P. eds, ASP Vol. 117, p.28
 Dubinski J., Carlberg R., 1991, *ApJ* 378, 496
 Gingold R.A., Monaghan J.J., 1977, *MNRAS* 181, 375
 Giraud E., 2000, *ApJ* 531, 701
 Hernquist L., 1990, *ApJ* 356, 359
 Hernquist L., Katz N., 1999, *ApJS* 70, 419
 Hollenback D., McKee C.F., 1979, *ApJS* 41, 555
 Huss H., Jain B., Steinmetz M., 1999, *ApJ* 517, 64
 Jing Y.P., Suto Y., 2000, *ApJ* 529, L69
 Katz N., 1992, *ApJ* 391, 502
 Lia C., Carraro G., 2000, *MNRAS* 314, 145
 Loewenstein M., White III R.E., 1999, *ApJ* 518, 50
 Lucy, L., 1977, *AJ* 82, 1013
 Mateo M., 1998, *ARA&A* 36, 435
 Miller G. E., Scalo J. M., *ApJS* 41, 513
 Moore B., Governato F., Quinn T., Stadel J., Lake G., 1998, *ApJ* 462, 563
 Navarro J.F., Frenk C.S., White S.D.M., 1996, *ApJ* 462, 563
 Persic M., Salucci P., Stel F., 1996, *MNRAS* 281, 27
 Press W. H., Flannery B. P., Teukolsky, S. A., Vetterling, W. T., *Numerical Recipes*, 1989, Cambridge: Cambridge University Press
 Salucci P., Persic M., 1997, in "Dark and Visible Matter in Galaxies", Persic M. & Salucci P. eds, ASP Vol. 117, p.1
 Steinmetz M., Müller E., 1993, *A&A* 268, 391
 Sutherland R. S., Dopita M. A., 1993, *ApJS* 88, 253
 Syer D., White S.D.M., 1998, *MNRAS* 293, 337
 Swaters R., 1999, PhD Thesis, Groningen University
 Thacker R.J., Tittley E.R., Pearce F.R., Couchman H.M.P., Thomas P.A., 1998, ([astro-ph/9809221](#))
 Thornton K., Gaudlitz M., Janka H.-Th., Steinmetz M., 1998, *ApJ* 500, 95
 Van den Bosch, Robertson J.J., de Block W.J.G., 2000, ([astro-ph/9911372](#))
 Weil M.L., Eke V.R., Efstathiou G., 1998, *MNRAS* 300, 773

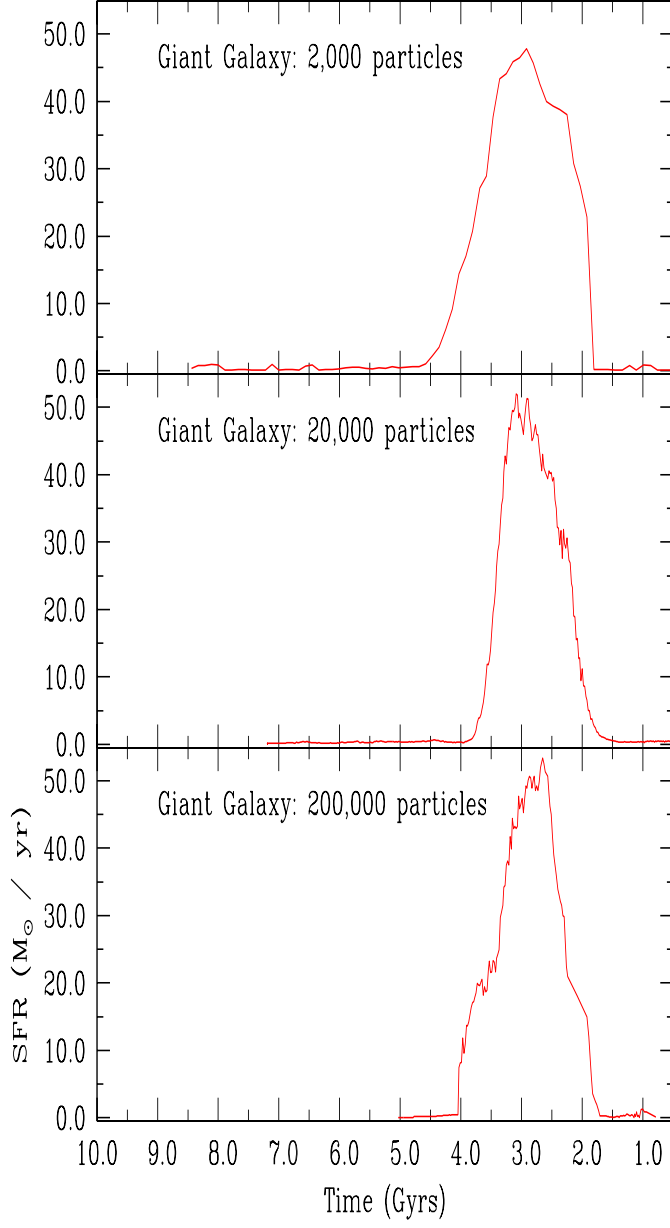


Fig. 2. SF for the giant elliptical as a function of time. From the top to the bottom the same model is shown at increasing number of particles, i.e at increasing resolution.

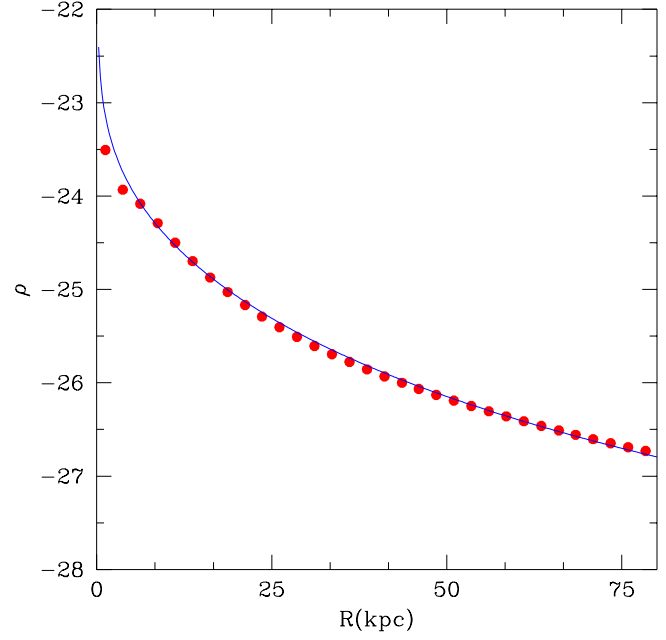


Fig. 3. Final stellar density profile of the giant galaxy. Over-imposed is a Hernquist profile for $r_e = 30 \text{ kpc}$.

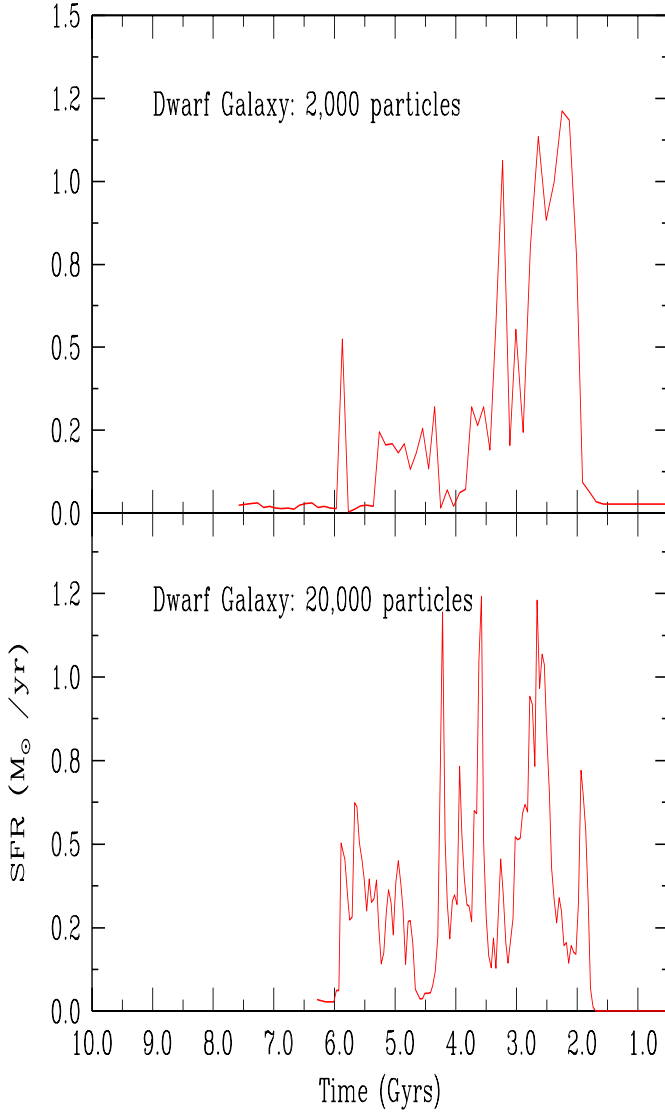


Fig. 6. SF history for the dwarf elliptical as a function of time. The two panels show the same model at increasing number of particles.

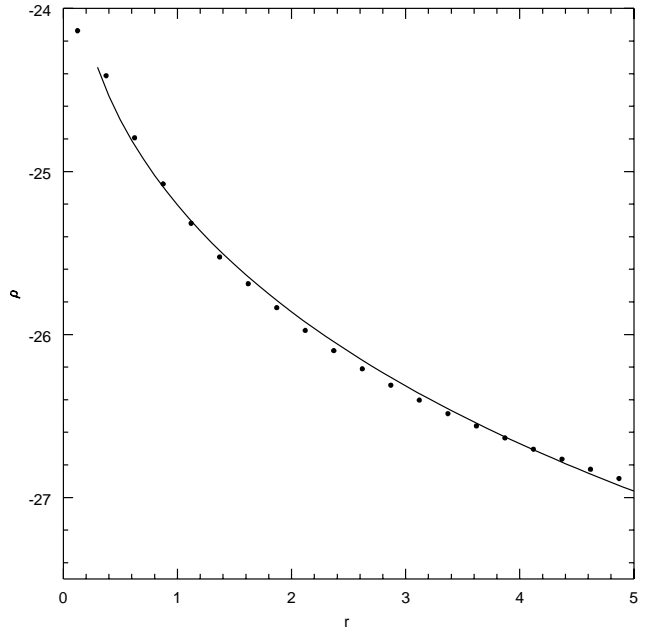


Fig. 7. Baryons final density profile. Overimposed is a Hernquist profile for $r_e = 2.8$ kpc.

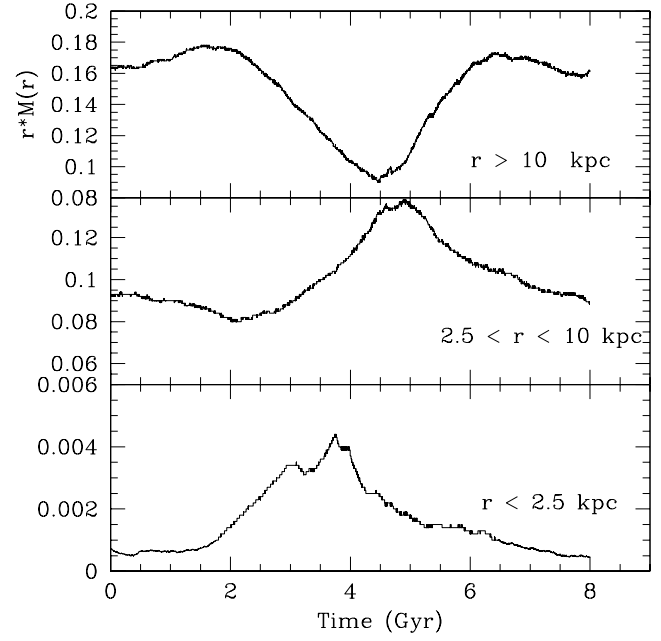


Fig. 8. Adiabatic invariant evolution for the dwarf galaxy in three different galaxy regions. $r \times M(r)$ is in code units.